Monte Carlo Simulation of Short Chain Branched Polyolefins in the Molten State

Javier Ramos,[†,‡] Loukas D. Peristeras,[†,§] and Doros N. Theodorou*[,†]

Department of Materials Science and Engineering, School of Chemical Engineering, National Technical University of Athens, 9 Heroon Polytechniou Street, Zografou Campus, 15780 Athens, Greece and Department of Macromolecular Physics, Instituto de Estructura de la Materia, CSIC, Serrano 113 bis, 28006 Madrid, Spain

Received July 19, 2007; Revised Manuscript Received October 13, 2007

ABSTRACT: Short chain branched (SCB) polyolefins as a model of metallocene ethylene/α-olefin copolymers were simulated by Monte Carlo (MC) and molecular dynamics (MD) methods. Melt density, which was evaluated by MD in the isothermal−isobaric ensemble (NPT−MD), slightly increases with the SCB content. A mix of different MC moves was adopted and connectivity-altering moves, such as end-bridging, were modified in order to incorporate the branches into the simulation. This MC simulation strategy performed very well in equilibrating molten SCB copolymers at all length scales. The chain size and local packing in the melt, as obtained from the MC simulations, are discussed. At given backbone length, chain size, as quantified by the radius of gyration, decreases with the number of branches. On the other hand, the presence of short branches leads to a less effective intermolecular local packing in the melt. Rheological properties of the copolymers are discussed based on a mapping of the Monte Carlo atomistic simulations on the packing length model, and compared with experimental results. In general, good agreement with experimental results is found.

1. Introduction

Nowadays, polyolefins are among the most important commodity plastics due to their low production costs and very wide range of applications. Commercial linear low-density polyethylenes are typically copolymers of ethylene and an α-olefin. Usually, 1-butene, 1-hexene, or 1-octene is used as the α-olefin comonomer, producing short chain branched (SCB) polymers[1] with two, four, or six carbon long branches, respectively. Random ethylene/α-olefin copolymers obtained by homogeneous single-site catalysts show a homogeneous comonomer distribution and a narrow molecular weight distribution (MWD), in contrast to traditional Ziegler−Natta catalysts.[2] In addition, by changing the structure of the single-site catalyst one can control the polymer molecular weight, the amount and distribution of the comonomer in the polymer backbone.[3,4] These polymerization methods make it possible to synthesize well-controlled polyolefin architectures which can be used as models for flexible polymers. Thus, it is an important issue to establish relationships between the macromolecular architecture and physical properties of these random copolymers.

Fetters et al. have studied the melt chain dimensions of poly(ethylene-co-1-butene) copolymers using small-angle neutron scattering (SANS).[5] They reported that the $\langle R^2\rangle_o/M$ parameter, where R is the end-to-end distance and M the molar mass, decreases monotonically as the ethyl branch content is increased. This experimental fact is in close agreement with rotational isomeric state (RIS) model calculations for branched polyethylenes, which showed that the radius of gyration decreases substantially as the number of ethyl branches is increased.[6] Later on, a combined MD/RIS study of ethylene/α-olefin copolymers was published by Madkour et al.[7] The characteristic ratio for these copolymers shows roughly two regions as a function of the comonomer content: (i) in copolymer chains containing mostly ethylene units (low comonomer content), the α-olefin suppresses the trans ethylene sequences, decreasing the characteristic ratio and (ii) as the comonomer content in the copolymer increases further, the characteristic ratio grows due to the adoption of helical sequences, which are lower in energy than all-trans ones. Experimentally, the same two regions have been found by comparing the SANS-derived chain dimensions for a wide range of branched polyolefins.[8] An empirical correlation has been developed for the dimension of the chains with a simple parameter characteristic of the chemical structure, the so-called molecular weight per backbone bond (m_b). Thus, the characteristic ratio (C_∞) reaches a minimum when half of the polymer is in the backbone and the other half is in the branches (for $m_b \approx 28$ g/mol); after this point, the characteristic ratio increases monotonically.

The research group of J. K. Maranas has studied computationally the dynamical behavior of small polyolefin chains containing regular branches.[9,10] They showed that, over the length scales of intermolecular packing, important differences appear between different chemical architectures. For example, for a highly branched polymer such as poly(isobutylene) (PIB), neighboring chains cannot pack well together. However, for less branched poly(butadiene) (PB), the intermolecular packing is more efficient, resembling that found in PE.

Some authors have developed empirical models that relate the degree of entanglement in the molten polymer to the dimension of the chains.[11−16] Among these models, one of the most popular is the packing length model.[14−16] In this model, the ratio of the occupied volume per polymer chain and the mean square radius of gyration of the polymer is defined as a packing length l_p ($l_p = V_{occupied}/\langle R_g^2\rangle$). This parameter is not dependent on the polymer molecular weight and thus is a

* Author to whom all correspondence should be addressed. E-mail: doros@chemeng.ntua.gr.

† Department of Materials Science and Engineering, School of Chemical Engineering, National Technical University of Athens.

‡ Department of Macromolecular Physics, Instituto de Estructura de la Materia, CSIC, Madrid, Spain. E-mail: j.ramos@iem.cfmac.csic.es. Telephone: +34915616800 (Ext: 3112).

§ E-mail: loukas.peristeras@scienomics.com. Present address: Scienomics, 17, Square Edouard VII, 75009 Paris, France.

10.1021/ma071615k CCC: $37.00
Published on Web 11/29/2007

constant attribute of the chemical architecture of the polymer. It has been empirically found that the packing length is related to important rheological properties.[8,16]

Within this framework, molecular simulations are reliable techniques for the determination of molecular structure, chain dimensions and thermodynamic properties. However, polymer systems are characterized by very long relaxation times that are hardly accessible by brute-force MD. On the contrary, MC simulations have been shown to be very efficient for the equilibration of long polymer chains at all length scales.[17] For example, the concerted rotation move (CONROT), which displaces five backbone segments and modifies eight consecutive torsion angles, is very effective in relaxing internal degrees of freedom in a chain.[18] The end-bridge move (EB) changes the conformation of two different chains, bringing about relaxation at long-length scales. This move introduces some polydispersity in the system, which is controlled by formulating it in a semigrand canonical ensemble.[19] In addition, the configurational bias (CB) move allows the relaxation of a few segments (usually 4−7 monomers) from the end of the chains. The combination of these moves along with other simpler moves, such as reptation and flip moves, makes possible the relaxation of important structural quantities, such as the end-to-end distance and the radius of gyration.

Finally, hierarchical approaches must be adopted in order to overcome the long length and time equilibration scales in polymer systems. Atomistic simulations can be used to derive input for mesoscopic approaches in order to calculate physical properties governed by broad length and time scales.

First of all, in this paper, the melt density is calculated as a function of the branch content by NPT MD simulations. Subsequently, we investigate the performance of connectivity-altering MC moves in the equilibration of short chain branched polymers. Polymer dimensions as a function of the branch content are calculated using MC simulations. Next, a hierarchical approach is used, which maps the atomistic simulation results onto the packing length model. Predictions from the hierarchical approach are discussed in the light of experimental evidence on rheological properties available in the literature.

2. Simulation Methods and Molecular System

In the present work, short chain branched (SCB) polyethylenes as a model of ethylene/α-olefin copolymers were simulated. The average length in the backbone was C_{1000} for all models. Six models were simulated, containing different amounts of branches (0, 19, 46, 55, 100, and 115 branches/1000 C), placed randomly along the backbone. The branch length was four carbon atoms (C_4). An equal probability of head-to-head and head-to-tail comonomer additions is assumed during ethylene/1-hexene copolymerization leading to formation of the chains. The number of chains in the primary simulation box was 20. In all simulations, temperature and pressure were 450 K and 1 atm, respectively.

2.1. Molecular Model. A united atom model with methyl ($-CH_3$), methylene ($-CH_2-$) and methyne ($-CH-$) groups represented as individual interaction sites is used in this work. Nonbonded interactions are modeled by a 12−6 Lennard-Jones potential. Attractive tail-corrections are taken into account through direct integration.[20] The bending potential is represented by a harmonic form, while the torsional potential is modeled through a four-term cosine Fourier expansion. Adjacent sites along the chain are kept at a fixed distance of 1.54 Å. All parameters used in this work are taken from the TraPPE force field.[21] This force field has been applied successfully to calculate volumetric properties of linear and triarm star polyethylene models in our group.[22,23]

2.2. Molecular Dynamics Details. Molecular dynamics simulations have been undertaken with the main objective of studying melt dynamics directly. From these simulations, only densities are discussed here. Dynamical results will be reported in a forthcoming publication. The molecular dynamics simulations are carried out under constant pressure and temperature (NPT ensemble), which was implemented via the Nosé-Hoover Langevin piston method.[24] The simulation box comprises 20 chains, each consisting of 1000 backbone sites and a variable number of C_4 branches, as specified above. The equations of motion are integrated with the velocity Verlet method. To speed up the MD simulation, a multiple time step algorithm is used, namely the reversible reference system propagator algorithm (rRESPA).[25,26] This algorithm decouples slow and fast degrees of freedom using different Liouville operators for each, allowing the use of more than one time step for the time integration of the different degrees of freedom. Here, we used a $\delta t = 1$ fs for the bending and torsional potential and $\Delta t = 5$ fs for nonbonded interactions. The overall simulation time was 3 ns. This simulation time was found sufficient to equilibrate the volume of the simulation box and hence to calculate the density of the melt.

2.3. Generation of the Initial Structures. The generation of the initial structures at a given density is performed using a modified recoil growth algorithm with periodic boundary conditions.[27,28] The procedure is sketched in Scheme 1. Consider a system consisting of N_{ch} chains, each containing n monomers and b butyl branches. In the present implementation, chains are placed and built sequentially. The key point in the growing of chains is to generate structures with prescribed bending and torsion angle distributions. In order to accomplish this, the algorithm uses an effective size (σ_{eff}) parameter for the nonbonded interactions. The σ_{eff} is calculated following the method of Curco and Alemán,[28] in which σ_{eff} is set equal to the "real" σ times a scaling factor $\lambda < 1$. Thus, the generated structures have some nonbonded overlap between monomers with a "correct" distribution of bend and torsion angles. Subsequently, the overlapped structure is easily relaxed using a small number of MC steps (10^5-10^6 MC steps). In order to ensure a better efficiency in branched systems, two different λ values are defined, one for backbone atoms (λ_{bb}) and another for branch atoms ($\lambda_{br} < \lambda_{bb}$).[28] Values of $\lambda_{bb} = 0.650$, $\lambda_{br} = 0.550$ were used throughout this work. The overlap condition is based on the evaluation of the distance between the sites already placed (j) in the box and the current atom (i). If the distance between the i and j sites is smaller than $0.5(\sigma_{eff,i}+\sigma_{eff,j})$, the new position is labeled as nonfeasible.

The first monomer is randomly placed in the simulation box. After that the second and third monomers are placed using random Euler angles, taking into account the geometric constraints imposed by the fixed bond length between two adjacent monomers and the bending potential between triplets of linked monomers. If overlap is found, the three atoms are removed and rebuilt starting from a different point in the simulation box. The process described above is repeated until the position of the three atoms is accepted. Once the three first atoms for the current chain have been placed in the simulation box, the next atom in the current chain is built by generating k trial orientations ($k = 8$ in this work) for the bond, connecting it to the already built part of the chain according to the imposed bending and torsional potentials. Then, the algorithm checks the viability of each of the k trials by looking for overlaps with

Scheme 1. Schematic Representation of the Generation of the Initial Structures

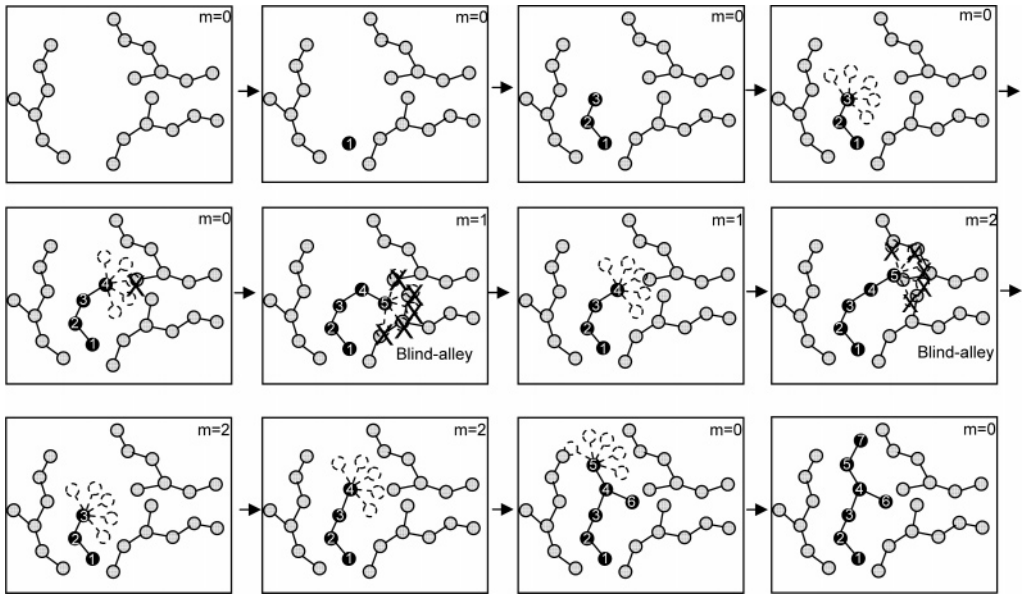

atoms already placed in the simulation box. The weight for each feasible trial is given by

$$w_i = \frac{\exp(-\beta E_{i,\text{torsion}} - \beta E_{i,\text{bend}})}{\sum_j \exp(-\beta E_{j,\text{torsion}} - \beta E_{j,\text{bend}})} \quad (1)$$

where $E_{i,\text{torsion}}$ is the torsional energy of the ith trial for the new monomer and β is $1/(k_B T)$. Subsequently, one of the feasible trials is chosen according to the above weights. If overlap is found for all k trials at monomer l ("blind-alley" condition), then the algorithm goes back to rebuild a segment of the chain ($l-m$ monomers). The length of this segment is given by the value of the parameter m, which initially is zero. The value of m increases by one whenever a "blind-alley" condition is detected; at the same time, the monomer l is marked. Eventually, at the moment that the chain reaches the marked monomer again, the parameter m is reset to zero. Branch atoms are placed as soon as they are encountered during the chain growth process. This procedure is repeated until all chains are situated in the simulation box. Subsequently, the overlapped structure is relaxed through 10^5-10^6 MC steps using the full potential.

2.4. Monte Carlo Simulations. A mix of reptation (5%), monomer flip (5%), SCB concerted rotation (15%), SCB end-bridge (50%), branch point move (10%), branch configurational bias (3%), and end configurational bias (12%) Monte Carlo moves were used for the equilibration of polymer chains. The semi-grand-canonical constant pressure ensemble ($NnPT\mu^*$) was used, which keeps the number of chains (N), the number of monomers (n), the temperature (T), and a profile of relative chemical potentials (μ^*) constant.[19] The microstructure of the SCB polymers was controlled using two uniform distributions, one for the number of branches in each chain and another for the number of carbon atoms between two consecutive branches (spacer atoms) within a chain. The number of branches in any chain is in the range $[\bar{B}(1-\Delta_B),\bar{B}(1+\Delta_B)]$, where $\bar{B}$ is the average number of branches per chain and Δ_B gives the reduced half-width of the distribution. A similar expression is used for the number of carbons between branches (spacer atoms); $[\bar{S}(1-\Delta_S),\bar{S}(1+\Delta_S)]$, where $\bar{S}$ is the mean number of mers between two branches in the chain and Δ_S gives, again, the reduced half-width of the distribution. A value of 0.5 was used in this work for both Δ_B and Δ_S. Unless noted otherwise, all Monte Carlo simulations consisted of runs of 600×10^6 MC steps.

Scheme 2. Schematic Representation of the Branch Configurational Bias Monte Carlo Move (br-CBMC)

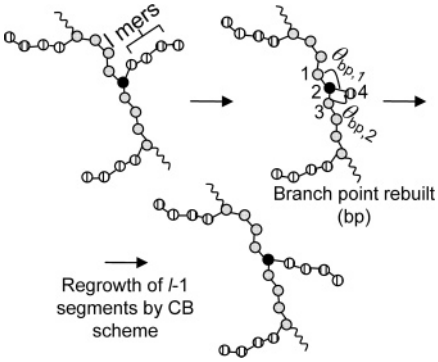

Monomer flip and branch point moves have been performed as they have been described in the literature.[23,29,30] However, the rest of the moves need some clarification when used in chains containing short chain branches (please see below).

The starting point for the derivation of the acceptance criterion of a Monte Carlo move is the microscopic detailed balance condition.[27] The transition from an old state (o) to a new state (n), provided all chain species involved in both states are feasible, can be written as

$$acc(o\rightarrow n) = \min\left(1, \frac{\alpha(n\rightarrow o)}{\alpha(o\rightarrow n)} \exp[-\beta(U^{\text{tot}}_{(n)} - U^{\text{tot}}_{(o)})]\right) \quad (2)$$

where $\alpha(o\rightarrow n)$ denotes the probability to attempt a move to the new state (n) from the old state (o), whereas $\alpha(n\rightarrow o)$ gives the probability of attempt for the reverse transition; $\beta = (1/k_B T)$ is the inverse thermal energy; and $U^{\text{tot}}_{(n)}$ and $U^{\text{tot}}_{(o)}$ are the unbiased total potential energy of the new and old states, respectively. The key step in order to get an acceptance criterion is to design analytical expressions for the α probabilities.

Reptation Move. This has been implemented as follows. A terminal backbone site of a randomly selected chain is cut off and appended to the other end with a randomly chosen torsion angle. In order to preserve the number of branches during this move, the number of spacer atoms between each end of the

chain and the branch point closest to this end is checked. If either number of spacer atoms is smaller than $\bar{S}(1 - \Delta_S)$ or greater than $\bar{S}(1 + \Delta_S)$, the move is rejected.

Branch Configurational Bias Monte Carlo (br-CBMC). This move allows equilibrating branches along the backbone polymer chain. The br-CBMC move consists of a combination of branch point rebuild (bp) for the first mer in the branch and configurational bias regrowth (br-CB) for the remaining ($l - 1$) monomers in the branch (see Scheme 2). Thus, the probability selection ratio may be written as

$$\frac{\alpha(n\rightarrow o)}{\alpha(o\rightarrow n)} = \frac{\alpha^{\mathrm{bp}}(n\rightarrow o)\prod_{l'=2}^{l}\alpha_{l'}^{\mathrm{br}}(n\rightarrow o)}{\alpha^{\mathrm{bp}}(o\rightarrow n)\prod_{l'=2}^{l}\alpha_{l'}^{\mathrm{br}}(o\rightarrow n)} \tag{3}$$

The bp monomer is rebuilt through a generation of k trials for the $\theta_{\mathrm{bp},1}$ and $\theta_{\mathrm{bp},2}$ bending angles (see Scheme 2). Afterward, the nonbonded energy is calculated for each trial. The probability ratio for the configuration selection is given by

$$\frac{\alpha^{\mathrm{bp}}(n\rightarrow o)}{\alpha^{\mathrm{bp}}(o\rightarrow n)} = \frac{W_{\mathrm{bp}}^{o\rightarrow n}\exp(-\beta V_{\mathrm{bp}}(o))}{W_{\mathrm{bp}}^{n\rightarrow o}\exp(-\beta V_{\mathrm{bp}}(n))} \tag{4}$$

where V_{bp} is the bias potential used in the move, which can be written as

$$V_{\mathrm{bp}} = \sum_{p=1,2} V^{\mathrm{bend}}(\theta_{\mathrm{bp},p}) + V^{\mathrm{LJ}}(\mathbf{r}_{\mathrm{bp}}) \tag{5}$$

W_{bp} denotes the Rosenbluth weight,[27] given by

$$W_{\mathrm{bp}} = \sum_{k'=1}^{k}\exp[-\beta V^{\mathrm{LJ}}(\mathbf{r}_{\mathrm{bp},k'})]\prod_{p=1,2}\exp[-\beta V^{\mathrm{bend}}(\theta_{\mathrm{bp,p},k'})] \tag{6}$$

Each of the remaining $l - 1$ segments in the branch is reconstructed by selection of a bending angle according to the Boltzmann factor of the bending potential. Subsequently, k trial directions for the added bond are randomly generated and nonbonded energies are calculated for each one. In this case, the probability ratio for the configuration selection is given by

$$\frac{\alpha_{l'}^{\mathrm{br}}(n\rightarrow o)}{\alpha_{l'}^{\mathrm{br}}(o\rightarrow n)} = \frac{W_{\mathrm{br},l'}^{o\rightarrow n}\exp(-\beta V_{\mathrm{br},l'}(o))}{W_{\mathrm{br},l'}^{n\rightarrow o}\exp(-\beta V_{\mathrm{br},l'}(n))} \tag{7}$$

where V_{br} and W_{br} are given by

$$V_{\mathrm{br},l'} = V_{l'}^{\mathrm{bend}}(\theta_{\mathrm{br}}) + V_{l'}^{\mathrm{LJ}}(\mathbf{r}_{\mathrm{br}}) \tag{8}$$

$$W_{\mathrm{br},l'} = \sum_{k'=1}^{k}\exp[-\beta V_{l'}^{\mathrm{bend}}(\theta_{\mathrm{br},k'}) - \beta V_{l'}^{\mathrm{LJ}}(\mathbf{r}_{\mathrm{br},k'})] \tag{9}$$

The acceptance criterion for the Br−CBMC move is obtained by application of the detailed balance condition as

$$acc^{\mathrm{br-CBMC}}(o\rightarrow n) = \min\left(1, \frac{J_{\mathrm{bp}}^{n}W_{\mathrm{bp}}^{o\rightarrow n}(\prod_{l'=2}^{l}W_{\mathrm{br},l'}^{o\rightarrow n})\exp[-\beta V^{\mathrm{tor},n}(\varphi_1,...,\varphi_l)]}{J_{\mathrm{bp}}^{o}W_{\mathrm{bp}}^{n\rightarrow o}(\prod_{l'=2}^{l}W_{\mathrm{br},l'}^{n\rightarrow o})\exp[-\beta V^{\mathrm{tor},o}(\varphi_1,...,\varphi_l)]}\right) \tag{10}$$

Scheme 3. Schematic Representation of the End Configurational Bias Monte Carlo Move (E-CBMC)

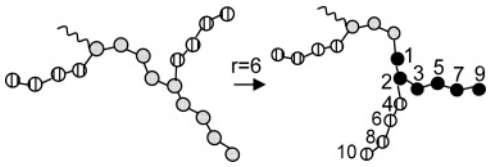

Scheme 4. Schematic Representation of the Concerted Rotation Move for SCB Polymers (SCB−Conrot)

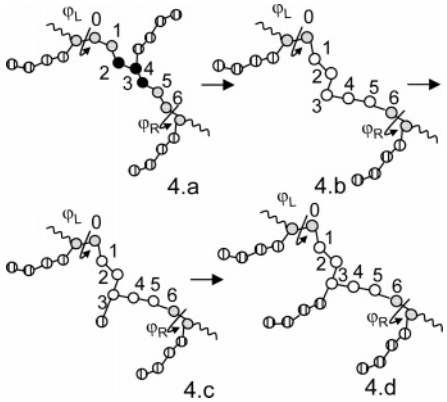

where J_{bp} denotes an appropriate Jacobian taking into account the change between Cartesian and constraint coordinate systems used in the branch point construction. The analytical expression for this Jacobian J_{bp} has been given as[23]

$$J_{\mathrm{bp}} = \frac{b^2\sin(\theta_{\mathrm{bp},1})\sin(\theta_{\mathrm{bp},2})}{[1 - \cos^2(\theta_2) - \cos^2(\theta_{\mathrm{bp},1}) - \cos^2(\theta_{\mathrm{bp},2}) + 2\cos(\theta_2)\cos(\theta_{\mathrm{bp},1})\cos(\theta_{\mathrm{bp},2})]^{1/2}} \tag{11}$$

where b and θ_2 stand for the bond length between atoms 2 and 4 and the bond angle formed by atoms 1, 2, and 3, respectively (Scheme 2).

The term $V^{\mathrm{tor},n}(\varphi_1,...,\varphi_l) = V^{\mathrm{tor},n}(\boldsymbol{\varphi}_{\mathrm{br}})$ includes all torsional energies for the l added segments, which have not been incorporated in the bias selection.

End Configurational Bias Monte Carlo (E-CBMC). The configuration of the chain ends is altered using this move. A chain end is randomly chosen, and then r backbone mers from the chain end are rebuilt using a configurational bias strategy. If a branch point is found during the chain regrowing, the branch and backbone mers are rebuilt one by one, in alternating fashion, using the same CB method. If a branch is found during this process, the reconstruction of the branch mers proceeds as described above in connection with br-CBMC. The algorithm is sketched in Scheme 3. The acceptance criterion for the CB move is available in the literature.[27]

Concerted Rotation Moves for SCB Polymers (SCB-CONROT). The concerted rotation move (CONROT) consists in the reconstruction of a randomly chosen internal sequence of mers along a chain by solving numerically[18] or analytically[31] the rebridging problem. However, in the case of SCB polymer chains, lateral branches have to be appropriately displaced in order to preserve the architecture of the polymer. Thus, the implementation of the CONROT move for SCB polymers is as follows (Scheme 4): (i) A monomer is randomly chosen and the bridge trimer segment is defined (Scheme 4.a). (ii) The φ_{L} and φ_{R} dihedrals are rotated, causing the monomers 1 and 5 to move. These rotations break the connectivity between 1 and 2

Scheme 5. Schematic Representation of the End Bridge Move for SCB Polymers (SCB-EB)

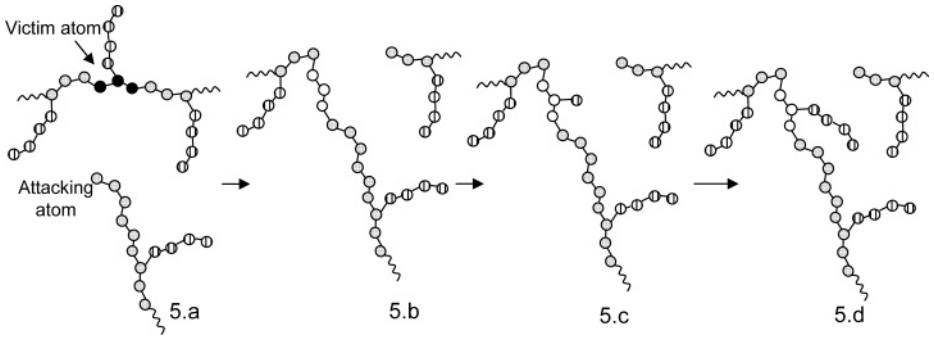

and 4 and 5 bonds. Reconstruction of bridge atoms (2, 3, and 4) by solving the bridging problem analytically is accomplished (Scheme 4b). (iii) If there is a branch attached to any bridge atom, this is rebuilt from the new bridge configuration using the br-CBMC move described above (Scheme 4, parts c and d). Then, the acceptance criterion can be written as

$$acc^{\mathrm{SCB-Conrot}}(o \rightarrow n) = \min\left(1, \frac{W_{\mathrm{bg}}^{\mathrm{tor},o\rightarrow n} J_{\mathrm{bg}}^{n} \exp(-\beta V^{\mathrm{LJ},n}(\mathbf{r}_{\mathrm{bg}}))}{W_{\mathrm{bg}}^{\mathrm{tor},n\rightarrow o} J_{\mathrm{bg}}^{o} \exp(-\beta V^{\mathrm{LJ},o}(\mathbf{r}_{\mathrm{bg}}))} \times \frac{J_{\mathrm{bp}}^{n} W_{\mathrm{bp}}^{o\rightarrow n} W_{\mathrm{br}}^{o\rightarrow n} \exp[\beta V^{\mathrm{tor},n}(\boldsymbol{\varphi}_{\mathrm{br}})]}{J_{\mathrm{bp}}^{o} W_{\mathrm{bp}}^{n\rightarrow o} W_{\mathrm{br}}^{n\rightarrow o} \exp[\beta V^{\mathrm{tor},o}(\boldsymbol{\varphi}_{\mathrm{br}})]}\right) \quad (12)$$

where bg, bp, and br labels stand for bridge atoms, first atom in the branch (branch point rebuilt), and branch atoms, respectively. The Jacobian J_{bg} can be expressed as[32]

$$J_{\mathrm{bg}} = \left|\frac{\mathbf{u}_6 \cdot \mathbf{e}_3}{\det(\mathbf{B})}\right| \quad (13)$$

where **B** is the matrix defined in ref 18:

$$\mathbf{B} = \begin{bmatrix} (\mathbf{u}_1 \times \mathbf{r}_{51}) & (\mathbf{u}_2 \times \mathbf{r}_{52}) & (\mathbf{u}_3 \times \mathbf{r}_{53}) & (\mathbf{u}_4 \times \mathbf{r}_{54}) & 0 \\ (\mathbf{u}_1 \times \mathbf{u}_6)\mathbf{e}_1 & (\mathbf{u}_2 \times \mathbf{u}_6)\mathbf{e}_1 & (\mathbf{u}_3 \times \mathbf{u}_6)\mathbf{e}_1 & (\mathbf{u}_4 \times \mathbf{u}_6)\mathbf{e}_1 & (\mathbf{u}_5 \times \mathbf{u}_6)\mathbf{e}_1 \\ (\mathbf{u}_1 \times \mathbf{u}_6)\mathbf{e}_2 & (\mathbf{u}_2 \times \mathbf{u}_6)\mathbf{e}_2 & (\mathbf{u}_3 \times \mathbf{u}_6)\mathbf{e}_2 & (\mathbf{u}_4 \times \mathbf{u}_6)\mathbf{e}_2 & (\mathbf{u}_5 \times \mathbf{u}_6)\mathbf{e}_2 \end{bmatrix} \quad (14)$$

with $\mathbf{u}_1$ to $\mathbf{u}_6$ being unit vectors along the six bonds of the heptamer, $\mathbf{r}_{ij}$ being the vector from atom i to atom j in the local numbering scheme used for the bridging construction, and $\mathbf{e}_1$ to $\mathbf{e}_3$ being the unit vectors of the global Cartesian coordinate system.

$W_{\mathrm{bg}}^{\mathrm{tor}}$ is a statistical weight associated with the torsional potential bias introduced in the bridge construction, being given by

$$W_{\mathrm{bg}}^{\mathrm{tor}} = \sum_i \exp[-\beta V^{\mathrm{tor}}(\phi_{\mathrm{bg},i})] \quad (15)$$

where index i runs over all solutions of the bridging problem.[18,22,23,32]

End Bridging Moves for SCB Polymers (SCB-EB). Similar to the above move, this move has three stages, as drawn in Scheme 5. The attacking atom is always a terminal backbone atom and the victim atom is always an unbranched backbone atom. After the move is performed, the attacking atom becomes an unbranched backbone atom, and this enables microscopic reversibility. Each chain has a fixed number—as opposed to location—of branches, until it takes part in a successful SCB-EB move. The acceptance for this move is given, after the detailed balance condition is applied, by

$$acc^{\mathrm{SCB-EB}}(o \rightarrow n) = \min\left(1, \frac{W_{\mathrm{bg}}^{\mathrm{tor},o\rightarrow n} J_{\mathrm{bg}}^{n} \exp(-\beta V^{\mathrm{LJ},n}(\mathbf{r}_{\mathrm{bg}})) N_{\mathrm{bg}}^{o}}{W_{\mathrm{bg}}^{\mathrm{tor},n\rightarrow o} J_{\mathrm{bg}}^{o} \exp(-\beta V^{\mathrm{LJ},o}(\mathbf{r}_{\mathrm{bg}})) N_{\mathrm{bg}}^{n}} \times \frac{J_{\mathrm{bp}}^{n} W_{\mathrm{bp}}^{o\rightarrow n} W_{\mathrm{br}}^{o\rightarrow n} \exp[\beta V^{\mathrm{tor},n}(\boldsymbol{\varphi}_{\mathrm{br}})]}{J_{\mathrm{bp}}^{o} W_{\mathrm{bp}}^{n\rightarrow o} W_{\mathrm{br}}^{n\rightarrow o} \exp[\beta V^{\mathrm{tor},o}(\boldsymbol{\varphi}_{\mathrm{br}})]}\right) \quad (16)$$

where N_{bg} denotes the number of candidate victims for the attacking end[19] and all other symbols have been explained above.

3. Results and Discussion

3.1. Density of the Copolymers as a Function of the SCB Content. NPT molecular dynamics (MD) simulations were performed to calculate the density of the polymer melt as a function of SCB content at 450 K and 0.1 MPa. As can be seen in Figure 1, the melt density slightly increases with the SCB content. However, only differences around 0.05 g/cm^3 are observed between the linear and the most branched polymer. The density obtained by our Monte Carlo simulations is within simulation error of the MD results. Furthermore, simulated densities agree well with available experimental data[33] within an error smaller than 1%.

3.2. Testing of Equilibration Methods in SCB Polymers. First of all, the CPU time required to run 30 million attempted moves is shown in Figure 2. The CPU time increases for the branched systems with respect to linear ones, mainly due to the introduction of additional elementary moves to equilibrate branches, such as br-CBMC and branch point moves, which are computationally expensive. On the other hand, the number of branches in the system does not affect the CPU time so much. The efficiency of the MC simulations in equilibrating long length scales for the SCB systems can be evaluated by examining the mean-square displacement of the chain center of mass (MSD−COM) and the end-to-end autocorrelation vector. As a prelude to this, we discuss the acceptance ratios for MC moves, which are given in Table 1. All MC moves present significant acceptance ratios except SCB-EB and BP moves, which exhibit acceptances lower than 0.2%. The acceptance ratio for flip, SCB−CONROT and SCB-EB moves decreases notably with the number of branches in the polymer chain, since they also involve a rearrangement of the branch atoms, as pointed out above. The mean-square displacements of the chain centers of mass (MSD−COM) are shown in Figure 3. This measure reflects the rate of generation of new chain configurations in terms of an effective chain motion.[34] The MSD−COM decreases

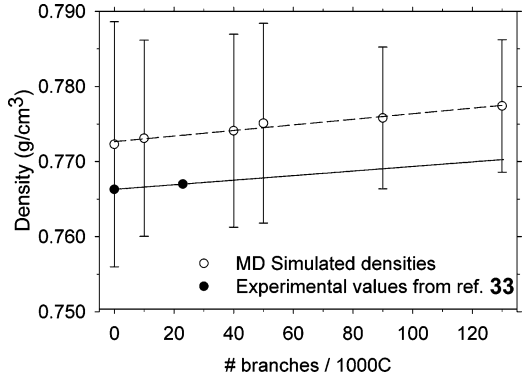

Figure 1. Melt density as a function of the short branch content at 450 K and 1atm from MD simulation. Experimental data for metallocene polymers are obtained from the Flory−Orwoll−Vrij equation of state in ref 33.

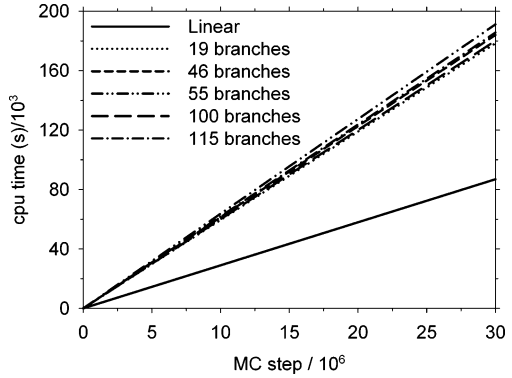

Figure 2. CPU time required as a function of the number of branches to run 30 million Monte Carlo attempted moves. All CPU times are on a dual Xeon single processor system at 3.0 GHz and 2.0 Gb of RAM memory.

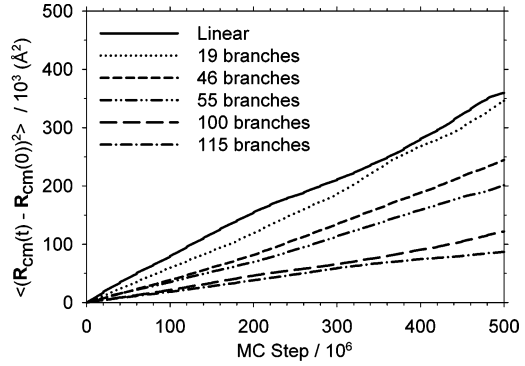

Figure 3. Center of mass mean squared displacement as a function of the MC step for each SCB polymer.

Table 1. Percent Acceptance of MC Moves for SCB Polymer Melts as a Function of the Number of Branches at 450 K and 1atm

av. no. of branches	rep	flip	SCB−CONROT	SCB-EB	BP	CB−SCB	CB-END
0	20.7	77.1	8.3	0.17			26.7
19	19.7	70.1	7.7	0.10	0.05	14.0	26.4
46	18.6	62.0	6.6	0.07	0.05	13.8	26.4
55	18.2	59.6	6.2	0.07	0.06	13.8	26.4
100	16.0	49.5	4.5	0.03	0.09	13.7	26.4
115	16.0	46.6	3.8	0.03	0.09	13.8	26.6

significantly as the number of branches increases in the melt polymer, showing a slow diffusion of the branched chains. This result is expected, as, when the number of branches increases, the acceptance of the EB move drops considerably. To quantify the rate of equilibration of the melt, one can count the number

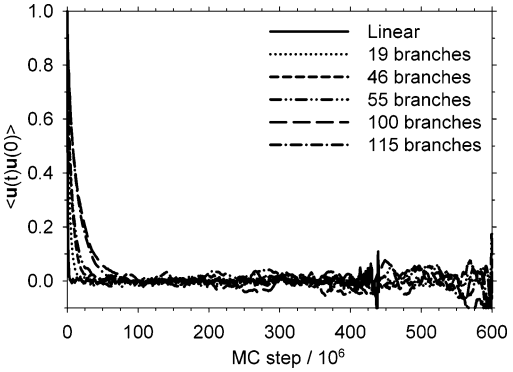

Figure 4. Autocorrelation function for the chain end-to-end vector with the number of MC steps for all SCB melt systems.

Table 2. Plateau Value for $\langle R^2(n)\rangle/n$ and Characteristic Ratio $C_\infty = (\langle R^2(n)\rangle/n)_{plateau}/l_0^2$ as a Function of the Branch Content[a]

av. no. of branches	m_b[b] (g/mol)	plateau $\langle R^2(n)/n$ (Å^2)	C_∞(sim)	C_∞(exp)[c]
0	14.0	20.0	8.4	7.4
19	15.1	19.0	8.0	7.1
46	16.6	18.3	7.7	6.9
55	17.1	17.9	7.5	6.8
100	19.6	17.0	7.2	6.6
115	20.5	17.3	7.3	6.5

[a] l_0 stands for the bond length which in this work has a value of 1.54 Å [b] Molar mass per backbone bond [c] This value has been calculated taking into account the empirical relationship between m_b and C_∞ ($C_\infty = 16.1 m_b^{-0.30}$ for 14 g/mol < m_b < 28 g/mol) proposed in reference 8.

Table 3. Relative Populations of Gauche and Trans States as Function of the Number of Branches

av. no. of branches	gauche$^+$ (%)	trans (%)	gauche$^-$ (%)
0	17.0	66.0	17.0
19	17.6	65.0	17.4
46	17.9	64.2	17.9
55	17.9	64.2	17.9
100	18.5	63.1	18.4
115	18.6	62.7	18.7

of steps needed for the end-to-end distance of the polymer to become equal to the MSD−COM.[22] For a linear system this number of steps needed is 3.3×10^6; for 19 branches per 1000 skeletal carbon atoms, it is 11.5×10^6; for 46 branches, it is 19.9×10^6; for 55 branches, it is 21.3×10^6; for 100 branches, it is 47.4×10^6; and for 115 branches, it is 51.8×10^6. The average effective displacement of the chains after 500×10^6 MC steps is in the range 600−335 Å, depending on the branch content. For comparison, the root mean squared chain end-to-end distances are on the order of 141−129 Å and the average radii of gyration are 58−53 Å, depending on the degree of branching (see Table 4 below). On the other hand, the autocorrelation function of the unit vector directed along the end-to-end vector for each SCB melt system is shown in Figure 4. As can be seen, the autocorrelation functions decay rapidly for all samples. After a determinate number of steps its value drops to zero, which is a measure of how fast the system forgets the long-range conformational characteristics of its initial configuration and, therefore, provides another measure of the effectiveness of the simulation method in equilibrating the chain conformations. It can be noted that the decay slows down as the number of branches increases. This happens because an abundance of branches in the polymer reduces the success rate of the end-bridge move. After $(80-100) \times 10^6$ MC steps, however, all systems are well equilibrated. Thus, the combination of MC moves proposed here works well with short chain branched polymers. This is a clear advantage of the connectivity-

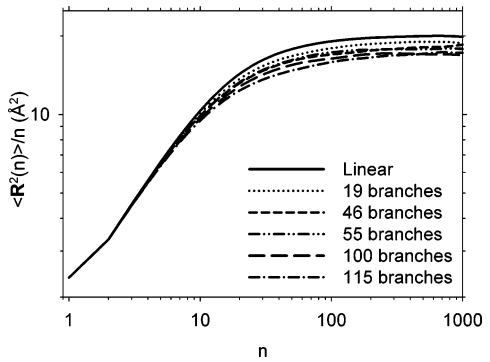

Figure 5. Equilibration of mean square internal distances for linear and short chain branched polymers.

altering MC method in comparison with conventional MD simulations, which are severely limited by the slow equilibration of these large-scale configurational features.

The mean-square internal distances between skeletal segments along the chains are studied in Figure 5. This function characterizes the equilibration of chain conformations at short and intermediate scales. A number of skeletal subchain lengths n, ranging from 1 to 1000 bonds, are considered. $\langle R^2(n)\rangle$ is the mean squared end-to-end distance over all subchains of length n in the melt. For well-equilibrated chains, $\langle R^2(n)\rangle/n$ increases monotonically and hyperbolically with the subchain length (n) and asymptotically reaches a plateau value.[35] This clearly happens in our simulations. The characteristic ratio of the subchains increases in the range of $1 < n < 30$, however for larger subchain lengths (in the range $n > 30$) it reaches a plateau value, which is characteristic of the nature of the chain microstructure of the various copolymers. The plateau value provides a measure of the conformational stiffness of the chain. As seen in Table 2, the stiffness decreases as the number of branches increases. This tendency is in good agreement with rotational isomeric state calculations (RIS) and empirical results for similar copolymers, which relate the characteristic ratio of molten polyolefins with the probability of occurrence of the comonomer units in the chain microstructure[7] and the molecular weight per backbone bond (m_b),[8] respectively. The larger values for our simulated characteristic ratios in comparison with experimental ones is likely attributable to the torsional potential used by the TraPPE force field throughout the simulations.[17]

3.3. Conformational Properties. Figure 6a shows the distribution of backbone dihedral (torsion) angles for all simulations. The corresponding populations of trans and gauche states, obtained as integrals of the distributions over the intervals between their minima, are given in Table 3. From these results, it is evident that the trans conformation population on the backbone bonds decreases as the number of branches increases; at the same time, both gauche$^+$ and gauche$^-$ states increase. On the other hand, Figure 6b represents the branch dihedral angle distributions for SCB polymers. This figure indicates that the branches are very rich in the trans conformational state and that the distribution of branch torsion angles is not significantly affected by the frequency of branches along the backbone.

3.4. Molecular Weight, Branch Number, and Interbranch Length Distributions. The linear melt polymer was controlled by imposing a uniform molecular weight distribution.[19] However, the architecture of the ethylene/1-hexene copolymer models was controlled by imposing two uniform distributions, one for the number of branches per chain and another one for the number of spacer atoms between two consecutive branches. For example, parts a and b of Figure 7 represent the simulated intermolecular and intramolecular branch distributions for the copolymer with 46 branches. All values have the same probability (within the statistical uncertainty), and simulation results are very close to the ideal uniform distributions. Thus, the elementary MC moves utilized result in uniform sampling of both the number of branches per chain and the number of mers between consecutive branches. The probability distribution of the number of mers of the polymer chain is shown in Figure 7c. The number of mers in each chain is steered by both branch distributions, therefore is not directly imposed during the simulation.

3.5. End to End Distances and Radii of Gyration. The mean square end to end distances $\langle R^2\rangle$ and radii of gyration $\langle R_g^2\rangle$ during the simulation are shown for all copolymers in Figure 8. After an initial equilibration period, both average end-to-end and radius of gyration distances reach constant values.

In Table 4, the values of $\langle R^2\rangle$, $\langle R_g^2\rangle$ and $\langle R^2\rangle/\langle R_g^2\rangle$ are collected as functions of the branch content in the copolymer. For all chain lengths and numbers of branches studied here, the random-coil relation $\langle R^2\rangle = 6\langle R_g^2\rangle$ is an excellent approximation for the equilibrium values of $\langle R^2\rangle$ and $\langle R_g^2\rangle$. In addition, the chain dimension decreases as the number of branches increases, except for the two most branched polymers, which seem to reach a plateau value, as shown in Figure 9 for $\langle R_g^2\rangle$ as a function of the number of branches. This plateau value is not evidenced in the $\langle R^2\rangle$ results, most likely because there are larger statistical uncertainties in the calculation of end to end distances. A comparison between the simulated and experimental chain dimensions is presented in Figure 10, where $\langle R_g^2\rangle/M$ is plotted as a function of the average molecular weight per backbone bond for both the present simulations and the SANS (small-angle neutron scattering) data for ethylene−1-butene copolymers.[8] Although there are slight deviations, the two sets of data show a similar trend with branch content.

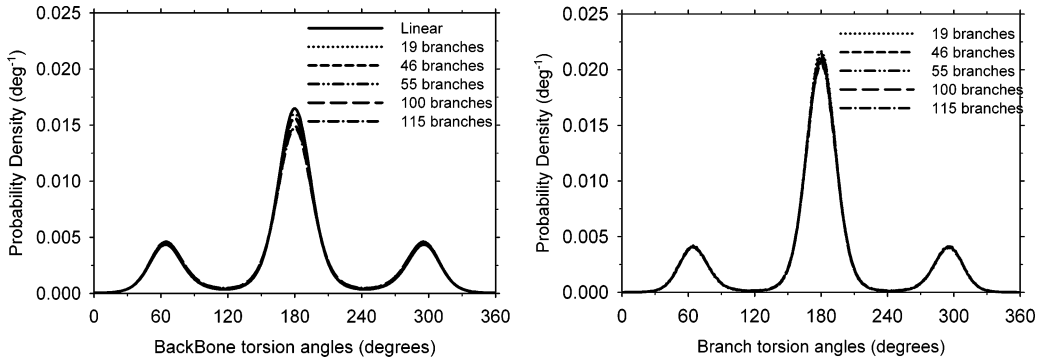

Figure 6. (a) Distribution of backbone torsion angles and (b) distribution of branch torsion angles for molten polymers of 1000 skeletal C atoms containing 0, 19, 46, 55, 100, and 115 C_4 branches.

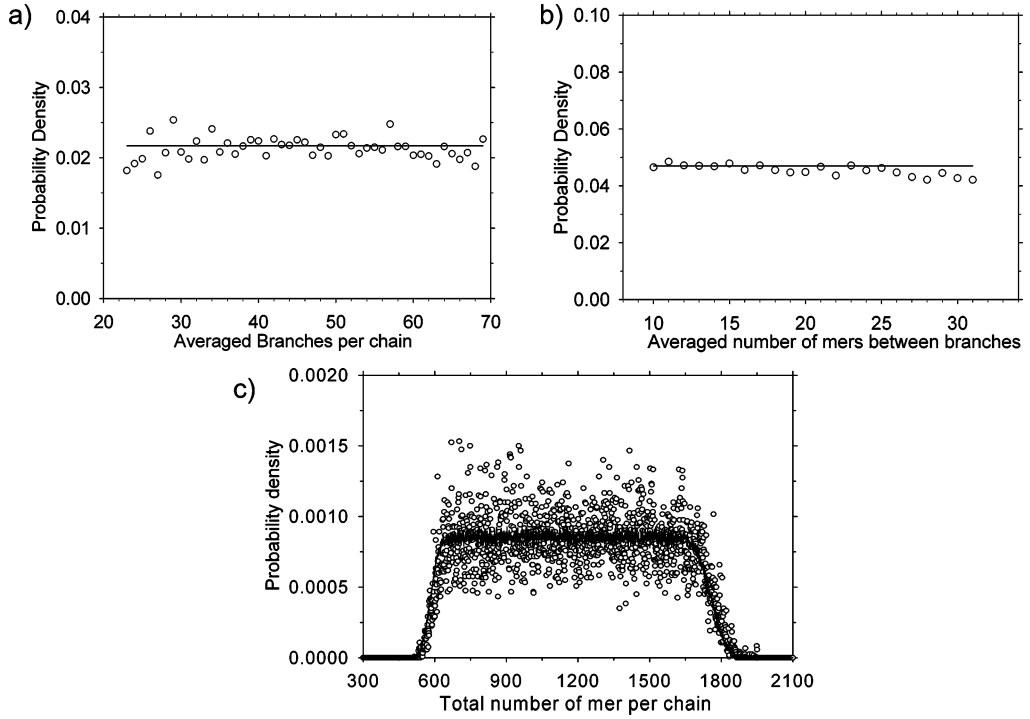

Figure 7. Probability distributions related to the microstructure of the copolymer containing 46 butyl branches. (a) Probability distribution of the number of branches of each polymer chain. The average number of branches is 46 and the minimum and maximum number of branches allowed is 23 and 69, respectively. (b) Probability distribution of the number of carbons between two consecutive branches. The average number of spacer atoms is 20 and the minimum and maximum number of spacer atoms is 10 and 30, respectively. (c) Probability distribution of the total number of monomers per chain. The lines correspond to the theoretically expected distributions.

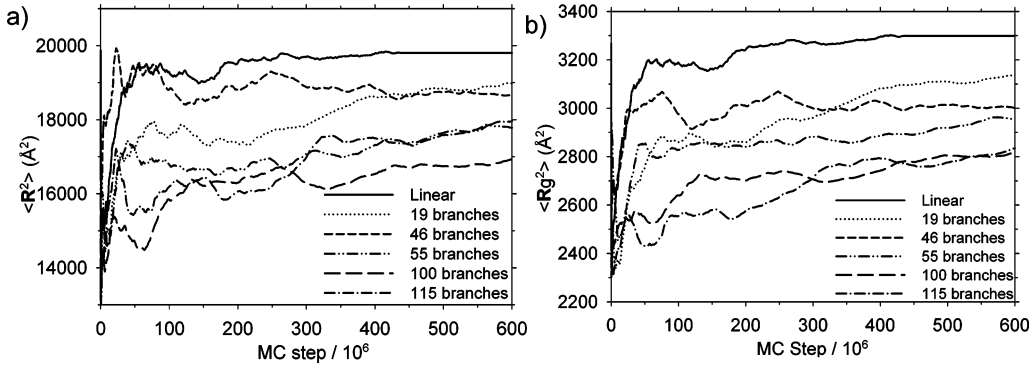

Figure 8. Average of the mean-square (a) end-to-end distance $\langle R^2 \rangle$ and (b) radius of gyration $\langle R_g^2 \rangle$ of the linear and SCB polymer melts.

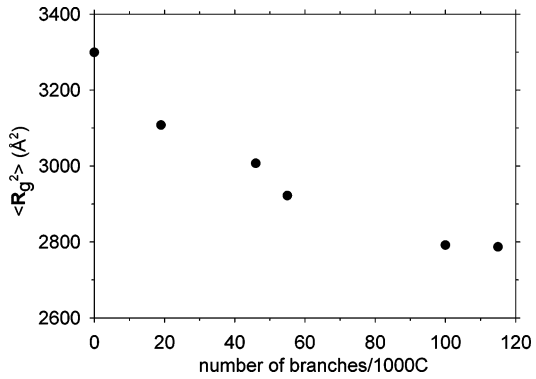

Figure 9. Mean square radius of gyration as a function of the number of branches in the polymer system.

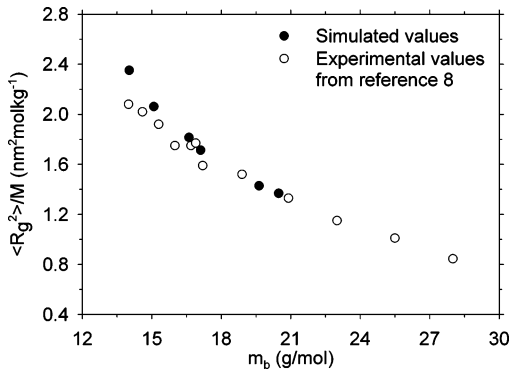

Figure 10. Calculated ratio $\langle R_g^2 \rangle / M$ for all model copolymers (full circles) and experimental $\langle R_g^2 \rangle / M$ for ethylene-1-butene copolymers as a function of the average molecular weight per backbone bond (m_b). Experimental values are taken from ref 8.

It is an interesting question whether helical conformations develop at high branch contents, as predicted by single-chain rotational isomeric state theoretical calculations; also, whether a minimum in $\langle R^2 \rangle$ and $\langle R_g^2 \rangle$ with respect to m_b exists, beyond which chain dimensions start rising again with branching. These questions are left for future simulation studies.

3.6. Local Packing. The local chain packing is used to characterize the order between different chains in the melt. This

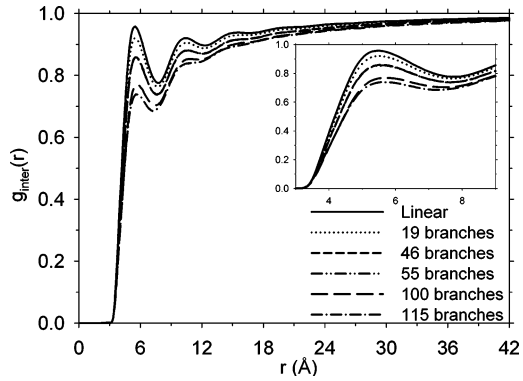

Figure 11. Intermolecular radial pair distribution functions for copolymers with varying branch content. The region 3−9 Å is magnified in the inset.

Table 4. Dependence of the Mean Square End-to-End Distances and Radii of Gyration on the Number of Branches in the Polymer Chain

av. no. of branches	$\langle R^2\rangle$(Å^2)	$\langle R_g^2\rangle$(Å^2)	$\langle R^2\rangle/\langle R_g^2\rangle$
0	19805 ± 50	3299 ± 6	6.00 ± 0.03
19	18795 ± 102	3108 ± 14	6.04 ± 0.06
46	18696 ± 58	3007 ± 6	6.22 ± 0.03
55	17602 ± 162	2922 ± 25	6.02 ± 0.11
100	16756 ± 68	2791 ± 17	6.00 ± 0.06
115	17596 ± 205	2787 ± 21	6.31 ± 0.12

can be described by the intermolecular pair distribution function, which quantifies changes in the local density of monomers belonging to different chains around a reference mer relative to the bulk density as a function of distance. Plotted in Figure 11 are the intermolecular pair distribution functions of the various branched polymers. The height of the nearest-neighbor peak is clearly affected by the degree of branching, indicating a less effective packing of chains as the number of branches increases. In addition, a shift to the right in the peak position with branch content is observed and shown in Table 5. Furthermore, one can observe a clear "correlation hole effect," $g_{inter}(r)$ being suppressed, relative to 1, over distances commensurate with the chain radius of gyration. The exclusion of segments coming from other chains at distances shorter than R_g becomes stronger as the number of branches increases. It has to be noted that, while not shown in Figure 11, $g_{inter}(r) \approx 1$ (universal behavior of a monatomic fluid) at distances larger than the radius of gyration of the polymer chains.

3.7. Mapping of Atomistic Simulation Results on the Packing Length Model. The packing length model links the size of polymer coils to the degree to which they entangle and, therefore, to their rheological behavior in the melt. The packing length is defined as the occupied volume (i.e., volume per polymer molecule) divided by the mean square end-to-end distance (squared chain size, proportional to the $^2/_3$ power of the pervaded volume) of a chain:[5,8,16]

$$p = \frac{V_{occ}}{\langle R^2\rangle} = \frac{M}{\langle R^2\rangle \rho N_A} \tag{17}$$

or equivalently,

$$l_p = \frac{V_{occ}}{\langle R_g^2\rangle} = \frac{M/\rho N_A}{\langle R_g^2\rangle} \tag{18}$$

where M is the molar mass of the polymer, ρ is the melt density and N_A is Avogadro's number. As $\langle R^2\rangle = 6\langle R_g^2\rangle$, clearly $l_p = 6p$. Here we have adopted the use of l_p to facilitate a comparison with experimental measurements. Remarkably, the packing length is a constant characteristic of the chemical structure of the polymer, since both V_{occ} and $\langle R_g^2\rangle$ (by virtue of Flory's random coil hypothesis) are proportional to M.

Table 5. Interchain Spacing Distance, Defined as the Position of the Maximum of the First Peak of the Intermolecular Pair Distribution Function $g_{inter}(r)$ as a Function of Degree of Branching

av. no. of branches	r_{max} (Å)
0	5.35
19	5.50
46	5.55
55	5.60
100	5.69
115	5.78

Table 6. Packing Length as a Function of the Chain Architecture

av. no. of branches	m_b (g/mol)	l_p (Å)	p (Å)
0	14.0	9.1	1.52
19	15.1	10.3	1.72
46	16.6	11.8	1.97
55	17.1	12.3	2.05
100	19.6	14.8	2.47
115	20.5	15.3	2.55

The packing length can be related to the characteristic ratio C_∞, which is given by

$$C_\infty = \frac{\langle R^2\rangle m_o}{M l_0^2} = \frac{m_o}{l_p l_0^2 \rho N_A} \tag{19}$$

where m_o is the molar mass of a monomer repeat unit and l_0 is the skeletal bond length (1.54 Å throughout this work). The definition of m_o may be problematic for random copolymers. In those copolymers, m_o is taken as the average molar mass per bond m_b in order to take into account the chemical structure of the chain. Empirically, a correlation between the packing length and m_b has been reported, and it will be discussed below.[8]

Taking into account these relations, we mapped the equilibrated MC trajectories onto the packing length model. The results are shown in Table 6, and a comparison with experimental data[8] is plotted in Figure 12. First at all, the value of l_p for the linear PE polymer can be used as a reference value. The l_p calculated by direct mapping between Monte Carlo simulations and the packing length model (9.1 Å) is close to those obtained using topological analysis of linear polyethylene melts by using an entanglement network of primitive paths (9.2−9.9 Å)[36] and it is somewhat underestimated with respect to the experimental value reported by Lohse (10.2 Å).[8] On the other hand, the packing length increases as the number of branches (or equivalently as the m_b parameter) increases. Experimentally, it has been empirically found that packing length l_p is related to m_b as

$$l_p\,(\text{Å}) = 0.33 m_b^{1.29} \quad (\text{experimental}, T = 463\ \text{K}) \tag{20}$$

The agreement between experimental and simulation data is quite good, as can be seen in Figure 12. Furthermore, simulated fits to a power law expression, in the range of m_b considered here, are very close to experimental ones (compare eqs 20 and 21):

$$l_p\,(\text{Å}) = 0.27 m_b^{1.34} \quad (\text{simulation}, T = 450\text{K}) \tag{21}$$

A physical model for these relations has not been published yet. However, based on the Monte Carlo simulations discussed above, we can hypothesize that the increase of packing length is related to the exclusion of segments of chains from a reference

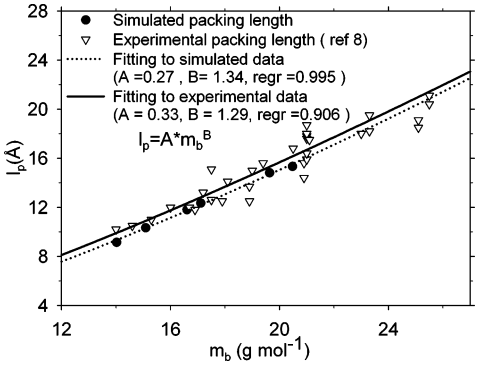

Figure 12. Packing length vs average molar mass per bond. Circles are calculated by mapping atomistic Monte Carlo trajectories on the packing length model and triangles are experimental values from ref 8. Solid and dotted lines correspond to the best fit to experimental and simulated values, respectively.

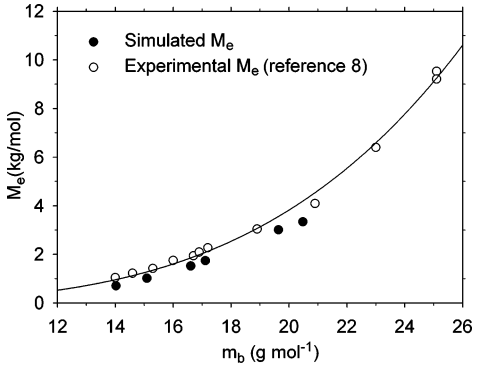

Figure 13. Simulated (filled circles) and experimental (open circles) entanglement molar mass as a function of the average molar mass per bond. Solid line corresponds to the best fit to experimental values from ref 8.

chain, as was discussed above in terms of the intermolecular pair-distribution function, and to changes in the size of chains in the melt as a function of the number of branches.

Rheological properties, such as entanglement molar mass (M_e) are related through the packing model.[14] Thus, it has been established that M_e is proportional to ρl_p^3, where the proportionality constant is independent of the temperature and polymer architecture:

$$M_e = 1.98 N_A \rho l_p^3 \quad (22)$$

Thus, in Figure 13, the M_e calculated from simulation values of ρ and l_p via eq 22 and some experimental data for flexible polymers[8] are plotted. The experimental and simulated values agree qualitatively. However, the simulated M_e is slightly underestimated in comparison with the experimental and other theoretical results. Again, we can use the value of the linear polyethylene as a reference. Experimentally, M_e values from 0.86 to 1.85 kg/mol have been reported.[8,15,37,38,39] These values were obtained from rheological experiments taking into account the relation $M_e = K\rho RT/G_N^o$, where G_N^o is the plateau modulus and K is a factor equal to 1[38,39] or 4/5.[8,15,37] Direct mapping via eq 19 yields a value of 0.71 kg/mol. At first glance, the quantitative differences between experimental and simulated M_e could be attributable to the torsional potential used here. Small deviations in l_p (or, equivalently, C_∞) lead to considerable errors in M_e, which depends on the third power of l_p. Karayiannis et al.[40] have reported a simulation value of $C_\infty = 8.0$ using an improved potential model for linear PE. Taking into account this value, the calculated entanglement molar mass is 0.88 kg/mol, which is within the M_e range of linear PE.

Finally, the increase in M_e with the degree of branching in the copolymers is in accordance with the intermolecular pair-distribution function discussed above. The local packing between chains is less effective when small branches are present, and therefore the number of entanglements decreases (or, equivalently, M_e increases). This qualitative picture is in agreement with the experimental observations for metallocene ethylene/1-hexene copolymers.[41]

4. Conclusions

In this work, a study of random ethylene/α-olefin copolymers in the melt state using Monte Carlo methods has been presented. A combination of Monte Carlo moves has been used. In order to take into account the short branches present along the backbones of polymer chains, some modifications of basic moves, such as concerted rotation and end-bridging, were needed. The SCB−Conrot (SCB-EB) move has been implemented as a combination of single concerted rotation (single end-bridging) move on the backbone atoms and subsequent regrowth of the short branch on the same atom using a configurational bias strategy. Furthermore, a branch point move based on the configurational bias technique (br-CBMC) has been implemented in order to relax the structure and the distribution of branches along the chains of the molten polymer. The combination of these Monte Carlo moves has been shown to equilibrate copolymer melts of high molecular weight. Although the relaxation of polymer chains is less effective as the number of branches increases, after 80−100 million MC steps all systems are well equilibrated at all length scales.

The distribution of trans/gauche bonds is altered by the presence of branches along the backbone. As the number of branches increases, the population of the trans conformation decreases for skeletal bonds. As a consequence, the size of the polymer chains decreases with the number of branches, reaching a plateau for the most branched systems examined here. Local packing in the melt is also affected by branching, showing a stronger correlation hole effect and a larger effective diameter for more branched chains. The most branched systems are locally denser than the less branched ones, making an efficient packing of chains in the melt more difficult. In general, as branching increases, other chains are excluded more strongly from the surroundings of a particular chain.

Finally, a mapping of the atomistic MC results on the packing length model has been performed. The packing length l_p, and hence the molar mass between entanglements M_e which can be correlated with it, increases with the number of branches. This result is in good agreement with experimental results obtained for polyolefins with different architectures and metallocene ethylene/1-hexene copolymers.

Acknowledgment. J.R. thanks the Ministerio de Educacion y Ciencia of Spain for financial support through a postdoctoral fellowship. Support to L.D.P. from the Greek Ministry of Education through a PYTHAGORAS-I program, co-funded by the European Social Fund (75%) and Greek national sources (25%) is gratefully acknowledged. The authors are grateful to Dr. David Curco for helpful discussions on the generation of the initial guess configurations. Very fruitful discussions with Dr. Juan Francisco Vega and Prof. Javier Martínez-Salazar are gratefully appreciated. The authors are also grateful to the Barcelona Supercomputing Center for allocation of CPU time on the MareNostrum supercomputer for the molecular dynamics simulations.

References and Notes

(1) Piel, C.; Starck, P.; Seppälä, J. V.; Kamminsky, W. *J. Polym. Sci., Part A: Polym. Chem.* **2006**, *44*, 1600.
(2) Mirabella, F. M. *J. Polym. Sci., Part B: Polym. Phys.* **2001**, *39*, 2800.
(3) Suhm, J.; Schneider, M. J.; Mülhaupt, R. *J. Mol. Catal. A* **1998**, *128*, 215.
(4) Cruz, V.; Ramos, J.; Muñoz-Escalona, A.; Lafuente, P.; Peña, B.; Martinez-Salazar, J. *Polymer* **2004**, *45*, 2061.
(5) Fetters, L. J.; Graessley, W. W.; Krishnamoorti, R.; Lohse, D. J. *Macromolecules* **1997**, *30*, 4973.
(6) Tonelli, A. E. *J. Am. Chem. Soc.* **1972**, *94*, 2972.
(7) Madkour, T. M.; Goderis, B.; Mathot, V. B. F.; Reynaers, H. *Polymer* **2002**, *43*, 2897.
(8) Lohse, D. J. *J. Macromol. Sci., Part C: Polym. Rev.* **2005**, *45*, 289.
(9) Neelakantan, A.; Maranas, J. K. *J. Chem. Phys.* **2004**, *120*, 465.
(10) Neelakantan, A.; Maranas, J. K. *J. Chem. Phys.* **2004**, *120*, 1617.
(11) Lin, Y. H. *Macromolecules* **1987**, *20*, 3080.
(12) Kavassalis, T. A.; Noolandi, J. *Phys. Rev. Lett.* **1987**, *59*, 2674.
(13) Colby, R. H.; Rubinstein, M. *Macromolecules* **1990**, *23*, 2753.
(14) Fetters, L. J.; Lohse, D. J.; Richter, D.; Witten, T. A.; Zirkel, A. *Macromolecules* **1994**, *27*, 4639.
(15) Fetters, L. J.; Lohse, D. J.; Graessley, W. W. *J. Polym. Sci., Part B: Polym. Phys.* **1999**, *37*, 1023.
(16) Fetters, L. J.; Lohse, D. J.; Milner, S. T.; Graessley, W. W. *Macromolecules* **1999**, *32*, 6847.
(17) Theodorou, D. N. *Mol. Phys.* **2004**, *102*, 147.
(18) Dodd, L. R.; Boone, T. D.; Theodorou, D. N. *Mol. Phys.* **1993**, *78*, 961.
(19) Pant, P. V. K.; Theodorou, D. N. *Macromolecules* **1995**, *28*, 7224.
(20) Dodd, L. R.; Theodorou, D. N. *Adv. Polym. Sci.* **1994**, *116*, 249.
(21) Martin, M. G.; Siepmann, J. I. *J. Phys. Chem. B.* **1999**, *103*, 4508.
(22) Mavrantzas, V. G.; Boone, T. D.; Zervopoulou, E.; Theodorou, D. N. *Macromolecules* **1999**, *32*, 5072.
(23) Peristeras, L. D.; Economou, I. G.; Theodorou, D. N. *Macromolecules* **2005**, *38*, 386.
(24) Feller, S. E.; Zhang, Y.; Pastor, R. W.; Brooks, B. R. *J. Chem. Phys.* **1995**, *103*, 4613.
(25) Tuckerman, M. E.; Berne, B. J.; Martyna, G. J. *J. Chem. Phys.* **1992**, *97*, 1990.
(26) Martyna, G. J.; Tuckerman, M. E.; Tobias, D. J.; Klein, M. L. *Mol. Phys.* **1996**, *87*, 1117.
(27) Frenkel, D.; Smit, B. *Understanding Molecular Simulations: From Algorithms to Applications*; 2nd ed.; Academic Press: New York, 2002.
(28) Curco, D.; Alemán, C. *J. Chem. Phys.* **2004**, *121*, 9744.
(29) Vacatello, M.; Avitabile, G.; Corradini, P.; Tuzi, A. *J. Chem. Phys.* **1980**, *73*, 548.
(30) Mavrantzas, V. G.; Theodorou, D. N. *Macromolecules* **1998**, *31*, 6310.
(31) Wu, M. G.; Deem, M. W. *J. Chem. Phys.* **1999**, *111*, 6625.
(32) Theodorou, D. N.; In Nielaba, P.; Mareschal. M.; Ciccotti, G. *Bridging Time Scales: Molecular Simulations for the Next Decade*; Springer-Verlag: Berlin, 2002, p 67.
(33) Han, S. J.; Lohse, D. J.; Condo, P. D.; Sperling, L. H. *J. Polym. Sci., Part B: Polym. Phys.* **1999**, *37*, 2835.
(34) Uhlherr, A.; Mavrantzas, V. G.; Doxastakis, M.; Theodorou, D. N. *Macromolecules* **2001**, *34*, 8554.
(35) Spyriouni, T.; Tzoumanekas, C.; Theodorou, D.; MullerPlathe, F.; Milano, G. *Macromolecules* **2007**, *40*, 3876.
(36) Tzoumanekas, C.; Theodorou, D. N. *Macromolecules* **2006**, *39*, 4592.
(37) Vega, J. F.; Rastogi, S.; Peters, G. W. M.; Meijer, H. E. H. *J. Rheol.* **2004**, *48*, 663.
(38) Raju, V. R.; Smith, G. G.; Marin, G.; Knox, J. R.; Graessley, W. W. *J. Polym. Sci., Polym, Phys. Ed.* **1979**, *17*, 1183.
(39) Raju, V. R.; Rachapudy, H.; Graessley, W. W. *J. Polym. Sci., Polym, Phys. Ed.* **1979**, *17*, 1223.
(40) Karayiannis, N. C.; Mavrantzas, V. G.; Theodorou, D. N. *Phys. Rev. Lett.* **2002**, *88*, 105503.
(41) Aguilar, M.; Vega, J. F.; J.; Sanz, E.; Martínez-Salazar, J. *Polymer* **2001**, *42*, 9713.

MA071615K